Extrusion-modulated DnaA activity oscillations coordinate DNA replication with biomass growth

Dengjin Li[1,2,5], Hai Zheng[1,2,5], Yang Bai[1,2,5], Zheng Zhang[1], Hao Cheng[1], Xiongliang Huang[1,2], Ting Wei[1,2], Arieh Zaritsky[4], Terence Hwa[3], Chenli Liu[1,2,] ✉

[1]Key Laboratory of Quantitative Synthetic Biology, Shenzhen Institute of Synthetic Biology, Shenzhen Institutes of Advanced Technology, Chinese Academy of Sciences, Shenzhen 518055, China. [2]University of Chinese Academy of Sciences, Beijing 100049, China. [3]Department of Physics & Department of Molecular Biology, University of California at San Diego, La Jolla, CA 92093-0319, USA. [4]Faculty of Natural Sciences, Ben-Gurion University of the Negev, Be'er Sheva, Israel. [5]These authors contributed equally: Dengjin Li, Hai Zheng, Yang Bai. ✉Email: cl.liu@siat.ac.cn

Abstract

Robust control of DNA replication is fundamental to bacterial proliferation. In *Escherichia coli*, replication initiation is thought to be regulated by oscillations in DnaA activity, driven by DnaA-chromosome interactions that differ among leading models. However, direct evidence linking these oscillations to replication initiation has been lacking, and existing models fail to explain the observed decoupling of replication initiation from *dnaA* expression. Here, we establish a direct link between DnaA activity and replication initiation by demonstrating robust oscillations in DnaA activity, which peak precisely at replication initiation across diverse growth conditions and genetic perturbations. Notably, these oscillations persist even when *dnaA* transcription remains constant, suggesting a regulatory mechanism that modulates DnaA activity independently of its expression. Additionally, we propose an extrusion model in which DNA-binding proteins sense biomass-DNA imbalance and extrude DnaA from the chromosome to trigger replication, overcoming limitations of existing models. Consistent with this model, perturbation of the nucleoid-associated protein H-NS modulates DnaA activity and replication timing, supporting its mechanistic validity.

Keywords: biomass-DNA coordination, chromosome replication initiation, DnaA activity oscillations, bacterial cell cycle

Introduction

Bacterial proliferation requires precise coordination between DNA replication and biomass growth to maintain cellular homeostasis. While biomass accumulates exponentially, DNA synthesis proceeds in a stepwise manner, creating temporal imbalances that demand continuous correction throughout the cell cycle (Fig. 1A-B). Failure to synchronize these processes risks catastrophic outcomes, such as growth defects, incomplete replication, unequal genetic segregation, and cell death (Boye et al., 1996; Khodursky et al., 2015; Lu et al., 1994; Mäkelä et al., 2024; Zaritsky & Pritchard, 1971). Central to this synchronization in *Escherichia coli* is the initiator protein DnaA, a DNA-binding protein that binds specifically to an asymmetric 9-bp DnaA-box, whose consensus sequence is TTWTNCACA (Hansen & Atlung, 2018; Speck et al., 1999). Although DnaA binding to the replication origin (*oriC*) triggers replication initiation (Dong et al., 2023; Kaguni, 2011; Ohbayashi et al., 2020; Ozaki & Katayama, 2012; Sekimizu et al., 1987), how DnaA activity is dynamically regulated to align replication initiation with cellular growth, particularly when DNA content and biomass diverge, remains a fundamental unresolved question in cell cycle biology.

Two competing models have dominated the field. The titration model posits that DnaA activity is governed by the availability of free DnaA, which accumulates until it surpasses the buffering capacity of chromosomal DnaA-boxes (Christensen et al., 1999; Hansen et al., 1991). Here, replication initiation resets the system by increasing DNA content (and thus DnaA-boxes), titrating excess DnaA. In contrast, the switch model emphasizes the ATP/ADP-bound states of DnaA: DnaA-ATP, synthesized during biomass growth, triggers initiation, while hydrolysis to DnaA-ADP following replication resets the cycle(Berger & Wolde, 2022; Donachie & Blakely, 2003; Fu et al., 2023; Hansen & Atlung, 2018; Katayama et al., 2017). Crucially, the titration model depends on ongoing DnaA synthesis to reflect biomass accumulation, whereas the switch model relies on nucleotide-state transitions, independent of total DnaA levels. Despite these mechanistic differences, both models consider that replication initiation is regulated by oscillations in DnaA activity, driven by DnaA-chromosome interactions (Fig. 1C). However, direct evidence linking these oscillations to replication initiation remains lacking. Moreover, neither model fully explains recent experimental observations: replication initiation persists for multiple generations even when *dnaA* transcription is completely inhibited (Knöppel et al., 2023). This discrepancy suggests an uncharacterized mechanism that senses biomass-DNA imbalance and directly modulates DnaA activity.

Here, using a synthetic reporter coupled with single-cell mRNA fluorescence *in situ* hybridization (FISH), we demonstrate that DnaA activity peaks precisely at initiation across diverse growth conditions and genetic backgrounds, even when *dnaA* transcription is held constant. DnaA activity oscillations persist independently of transcriptional feedback, pointing to a post-translational regulatory mechanism. We propose an extrusion model in which nucleoid-associated proteins (NAPs) sense biomass-DNA imbalance and dynamically extrude DnaA from the chromosome, liberating it to activate *oriC*. This model not only explains the decoupling of replication timing from *dnaA* expression but also integrates disparate experimental findings. Perturbations of the NAP, H-NS for instance, modulate DnaA activity and replication timing, directly supporting the model's predictions. By unifying regulatory principles across transcription, protein activity, and chromosome dynamics, our findings redefine the paradigm for bacterial replication control.

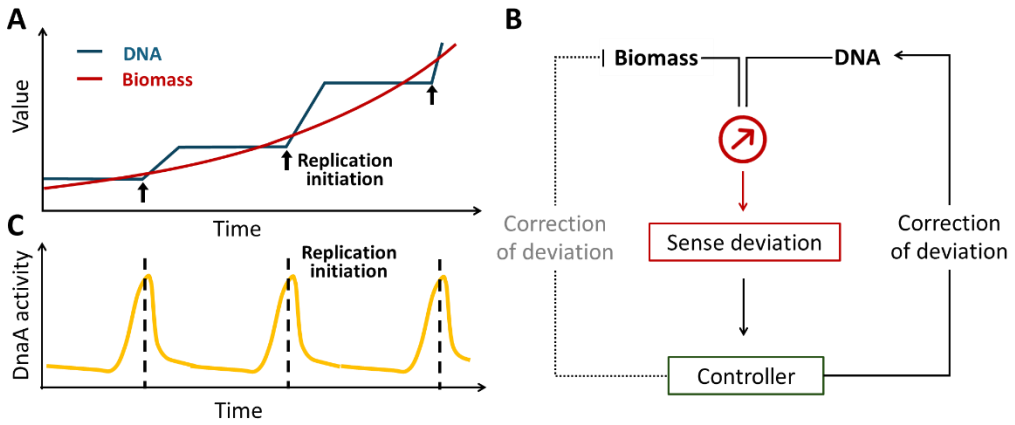

Figure 1. Coordination of biomass growth and DNA replication through replication initiation and DnaA activity oscillations. (A) Schematic representation of the discrepancy between biomass accumulation and DNA replication. While biomass grows exponentially, DNA synthesis progresses linearly, necessitating replication initiation events to maintain coordination. **(B)** Mechanistic model for biomass-DNA coordination in bacteria. A molecular sensor detects deviations between cell mass and DNA content, transmitting this information to regulatory controllers that compensate by either increasing DNA replication or restricting biomass accumulation. **(C)** Illustration of cyclic DnaA activity oscillations aligning with replication initiation to ensure precise cell cycle control.

Results

Development of a DnaA activity reporter system

It has been known that changing DnaA expression levels affects DnaA activity, and further changes initiation mass (Berger & Wolde, 2022; Løbner-Olesen et al., 1989; Zheng et al., 2020). To investigate this further, we engineered a *dnaA*-titratable strain, where *dnaA* transcription is controlled by an inducible P_{tet} promoter (Lutz & Bujard, 1997) (Fig. 2A). This system enabled precise modulation of *dnaA* mRNA levels (0.25 to 6 times the wild-type level) via anhydrotetracycline (aTc) induction (0.75–20 ng ml^{-1}) without altering growth rate or cell size (Fig. 2B–D). Strikingly, increasing DnaA expression doubled population-averaged *oriC* copy numbers and reduced initiation mass (the cell volume per *oriC* at replication initiation) by 50 % (Fig. 2E-F). The observed relationship between DnaA expression and initiation mass deviated significantly from both the titration and switch models (Fig. 2G), suggesting unaccounted regulatory mechanisms.

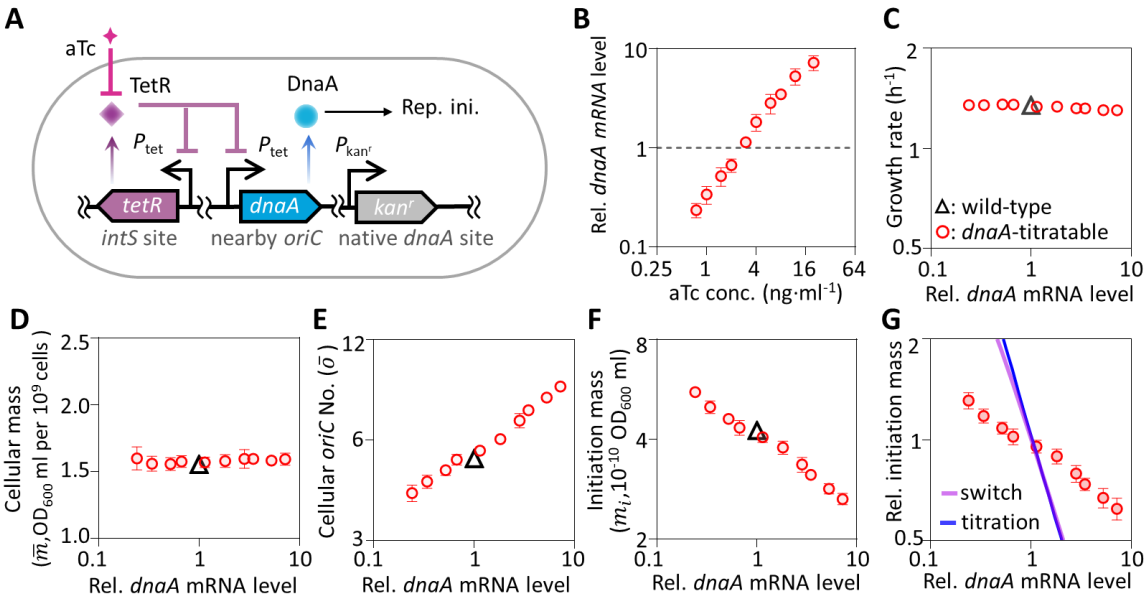

Figure 2. Construction and characterization of the *dnaA*-titratable strain. (A) Schematic of the *dnaA*-titratable strain. A *dnaA* gene under the control of the P_{tet} promoter was inserted near *oriC* and regulated by a P_{tet}-*tetR* feedback loop integrated at the *intS* locus, enabling fine-tuned expression control. The native *dnaA* gene was replaced with a kanamycin resistance cassette (*kan^r*). **(B–F)** Characterization of *dnaA*-titratable cells (red open circles) grown in rich defined medium with glycerol (M6) under varying aTc concentrations. Measured parameters include *dnaA* mRNA levels (**B**), growth rate (**C**), population-averaged cellular mass (**D**), population-averaged *oriC* numbers (E), and initiation mass (**F**). Wild-type MG1655 values (black triangles) are shown for comparison. *dnaA* mRNA levels, normalized to wild-type MG1655, increased with aTc concentration from 0.75 to 20 ng·ml^{-1}. Cellular mass was determined by OD_{600} divided by cell number concentration. *oriC* copy numbers were measured using a run-out assay, and initiation mass was calculated as the ratio of cellular mass to *oriC* numbers. Data represent means ± SD (n = 5 biological replicates). **(G)** Relationship between relative initiation mass and relative *dnaA* mRNA levels, compared with predictions from the initiation titration model (blue line) and the switch model (purple line). Experimental data are overlaid for validation.

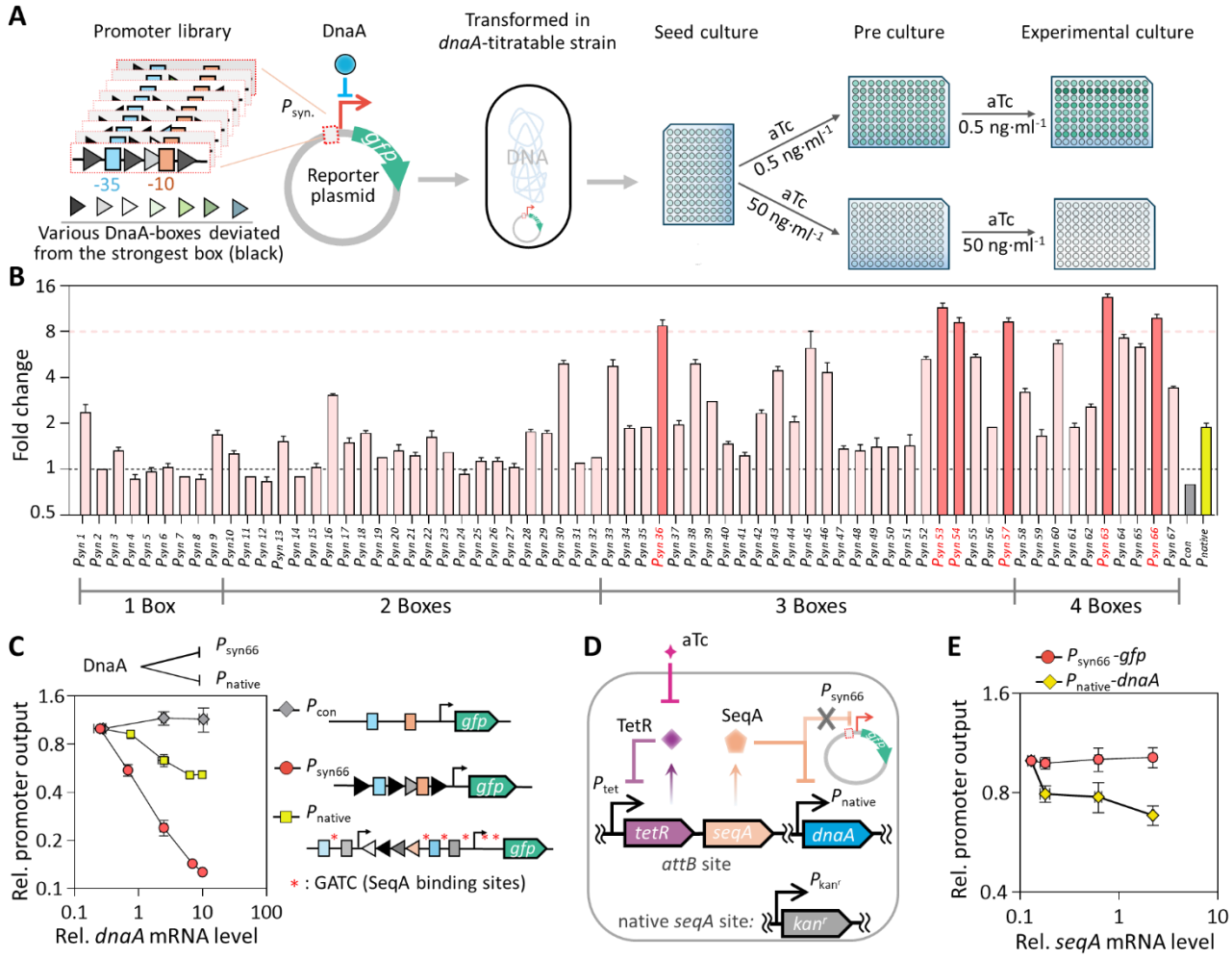

Figure 3. Development of a DnaA activity reporter system. (A) Schematic of promoter design and screening. Sixty-seven synthetic promoters were constructed by inserting various DnaA-boxes around the promoter core to drive *gfp* expression in a *dnaA*-titratable strain, where *dnaA* expression was regulated by aTc concentration. After pre-cultivation, GFP fluorescence per OD_{600} was measured using a microplate reader in cells grown under low (0.5 ng·ml^{-1}) or high (50 ng·ml^{-1}) aTc concentrations to determine repression fold-change. **(B)** Repression fold-change of synthetic promoters. P_{con} (a promoter lacking DnaA-boxes) and P_{native} (the endogenous *dnaA* promoter) served as negative and positive controls, shown in gray and yellow, respectively. **(C)** Response curves of three promoters to varying *dnaA* expression levels, with their promoter architectures shown on the right. Promoter activity was assessed by relative *gfp* mRNA levels, normalized to the lowest *dnaA* expression condition. Schematic **(D)** and response curves **(E)** of P_{syn66} and P_{native} responses to SeqA in the *seqA*-titratable strain. Promoter activity was quantified from *gfp* transcript levels in *seqA*-titratable cells containing the P_{syn66}-GFP plasmid, normalized to the lowest *seqA* expression level. All cells were grown in rich defined medium supplemented with glycerol across different aTc concentrations. Data represent mean ± SD from 3 biological replicates (**B**,**C**,**E**).

To dissect DnaA activity dynamics, we constructed a library of synthetic promoters (n = 67) by replacing *tetO* operators in P_{tet} with DnaA-boxes (Fig. S1). To assess the degree of DnaA activity-mediated repression, we measured the fold change in GFP expression driven by each synthetic

promoter under low and high levels of *dnaA* induction (Fig. 3A). Six synthetic promoters exhibited over 8-fold DnaA-mediated repression, whereas the promoter lacking DnaA-boxes (P_{con}) showed none, and the well-characterized native *dnaA* promoter (P_{native})(Braun et al., 1985; Saggioro et al., 2013; Speck et al., 1999) displayed approximately two-fold repression (Fig. 3B; Fig. S1). P_{syn66}, which contains three strong and one weak DnaA-box, exhibited >8-fold repression under high DnaA induction (Fig. 3B). P_{syn66}'s design enables responsiveness to both free DnaA levels (via strong boxes) and the ATP/ADP ratio (via differential binding to the weak box)(Grimwade & Leonard, 2021; Katayama et al., 2017; Speck et al., 1999). Dose-response assays confirmed that P_{syn66} was progressively repressed across a 40-fold range of *dnaA* expression (Fig. 3C), with no interference from SeqA-mediated sequestration (Fig. 3D-E). These results validated P_{syn66} as a robust and specific reporter of DnaA activity.

Decoupling DnaA activity oscillations from *dnaA* transcription fluctuations

To investigate DnaA activity dynamics throughout the cell cycle, we linked P_{syn66} activity to cell size, a surrogate for cell-cycle progression, using single-cell mRNA FISH(Skinner et al., 2013) to quantify *lacZ* mRNA levels in MG1655*Δlac* cells harboring the P_{syn66}-*lacZ* plasmid (Fig. 4A). A control strain harboring a promoter-less *lacZ* construct (P_{neg}) showed undetectable fluorescence signals (Fig. 4A), confirming the specificity of *lacZ* mRNA detection. Quantitative analysis revealed that P_{syn66}-driven mRNA levels fluctuated approximately 3-fold over the cell cycle, whereas the DnaA-unresponsive constitutive promoter (P_{con}) exhibited stable expression (Fig. 4B). However, fluctuations in mRNA concentration may not directly correspond to changes in DnaA activity due to global factors such as plasmid copy number and RNA polymerase concentration (Balakrishnan et al., 2022; Bintu et al., 2005a; Bintu et al., 2005b). To account for these variables, we used a P_{con}-*lacZ* plasmid to estimate global effects on mRNA concentration and calculated DnaA activity as inversely proportional to $k_{syn66} = \frac{[mZ](\mathrm{P_{syn66}})}{[mZ](\mathrm{P_{con}})}$. In wild-type cells (MG1655*Δlac*) harboring the synthetic reporter system (Fig. 4C), fluctuations in DnaA activity, as denoted by k_{syn66}^{-1}, displayed approximately a 3-fold variation across the cell cycle (Fig. 4D), underscoring the substantial cell cycle-dependent oscillations in DnaA activity.

We then examined whether the observed fluctuations in DnaA activity were linked to oscillations in *dnaA* transcription. Comparing the dynamics of *dnaA* mRNA and DnaA activity, we found that the peak in DnaA activity coincided with the trough in *dnaA* mRNA levels (Fig. 4D-E). To test whether *dnaA* transcription drives these oscillations, we eliminated transcriptional fluctuations using the *dnaA*-titratable strain. Despite constant *dnaA* mRNA levels (2 ng ml^{-1} aTc induction), DnaA activity was retained robust oscillations (Fig. 4F–H), demonstrating the decoupling of DnaA activity oscillations from transcriptional fluctuations. These suggest that post-translational regulation, not transcriptional feedback, governs the DnaA activity.

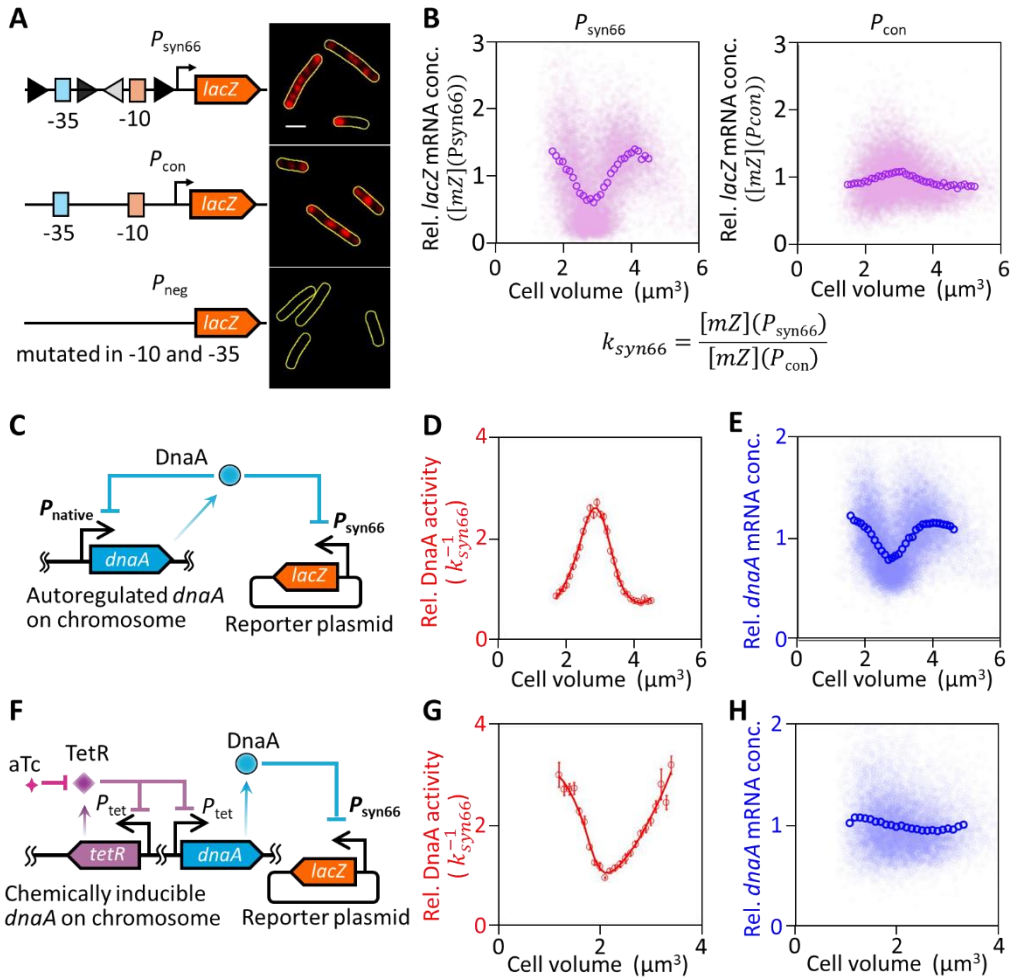

Figure 4. DnaA activity oscillations decoupled from *dnaA* transcription fluctuations. **(A)** Representative *lacZ* mRNA FISH images of MG1655 Δ*lac* cells transformed with *lacZ* expression plasmids driven by P_{syn66} (DnaA-boxes around promoter core), P_{con} (no DnaA-box around promoter core), or P_{neg} (mutated promoter core). Yellow outlines indicate cell boundaries identified from phase-contrast images. **(B)** Relative *lacZ* mRNA concentrations driven by P_{syn66} (left) and P_{con} (right) across different cell volumes. Relative concentrations were determined from volume-specific *lacZ* mRNA fluorescence intensities, normalized to the population average. Volume-binned data for P_{syn66} ($[mZ](P_{syn66})$) and P_{con} ($[mZ](P_{con})$) are shown as open circles and were used to calculate k_{syn66}. **(C)** Schematic of a strain with autoregulated *dnaA* transcription carrying a DnaA activity reporter plasmid. Cell cycle-dependent fluctuations in relative DnaA activity (**D**) and relative *dnaA* mRNA concentrations (**E**) in cells from panel **C**, grown in rich defined medium supplemented with glucose. Relative DnaA activity (k_{syn66}^{-1}), calculated from volume-binned data in panel **B**, was smoothed and plotted as a red curve (**D**). Relative *dnaA* mRNA concentrations were determined from volume-specific *dnaA* mRNA fluorescence intensities, normalized to the population average, with volume-binned data shown as open circles (**E**). (**F–H**) Same as panels **C–E**, but for cells with aTc induced *dnaA* transcription, grown in rich defined medium supplemented with glycerol under 2 ng·ml^{-1} aTc induction. More than 8,000 cells were analyzed per growth condition, and all error bars correspond to standard error of the mean (SEM).

DnaA activity oscillations are tightly coupled to replication timing

To explore the relationship between DnaA activity oscillations and DNA replication initiation, we examined cells grown under various nutrient conditions supporting different doubling times (30–66 min). Significant fluctuations in DnaA activity were observed across all conditions (Fig. 5A). We also estimated the cell volume at replication initiation (V_i) based on population-averaged cell volume and *oriC* number (Bremer et al., 1979; Si et al., 2017; Zheng et al., 2016) (Fig. S2 A–C), marking this on the DnaA activity profiles. In a representative birth-to-division cell cycle (Pountain et al., 2024) (Fig. S2D), DnaA activity peaks consistently coincided with V_i, indicating a close correlation between DnaA activity and replication initiation (Fig. 5A).

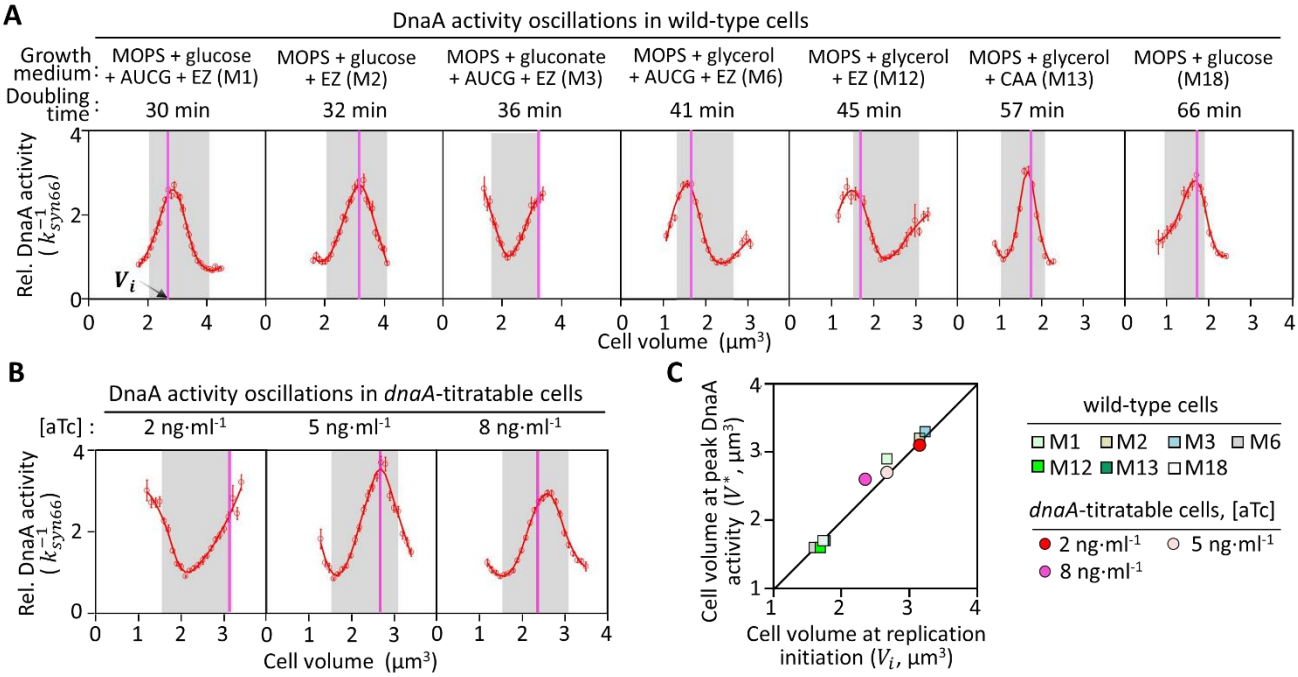

Figure 5. Tight correlation between DnaA activity oscillations and DNA replication initiation. (A) Cell cycle-dependent DnaA activity oscillations in wild-type cells across various growth conditions. DnaA activity is represented by k_{syn66}^{-1}. Volume-binned DnaA activity (red circles) was smoothed and plotted as a red curve. The representative birth-to-division cell cycle, defined as the cell volume doubling interval containing the majority of cells, is shaded in gray. The vertical line indicates the cell volume at replication initiation (V_i). **(B)** Cell cycle-dependent DnaA activity oscillations in *dnaA*-titratable cells grown in M6 medium with varying aTc concentrations. More than 8,000 cells were analyzed per growth condition, and error bars show the mean ± SEM. **(C)** Correlation between V^* and V_i in wild-type (squares) and *dnaA*-titratable (circles) cells. V^* represents the cell volume at the peak of DnaA activity within the representative birth-to-division cell cycle. The black line indicates equivalence between V^* and V_i.

Further genetic perturbations, such as titrating DnaA expression, shifted DnaA activity fluctuations, yet the relationship between V^* (the cell volume at maximal DnaA activity in a representative birth-to-division cell cycle) and V_i remained locked (Fig. 5B). To quantify this relationship, we compared V_i with V^*, revealing a strictly proportional relationship through the origin (slope= 1.0, R^2 = 0.98), indicating equivalence between V^* and V_i (Fig. 5C). These results confirm that DnaA activity

202 oscillations are tightly correlated with replication initiation, independent of transcriptional or
203 nutrient perturbations.

204 **An extrusion model reconciles paradoxical initiation events**

205 Very recently, Knöppel *et al.* reported that multiple rounds of initiation occurred even after DnaA
206 synthesis is shut down (Knöppel et al., 2023). In their experiment, DnaA was supplied in excess before
207 expression ceased (Knöppel et al., 2023), potentially allowing continued replication initiation due to
208 residual DnaA. To address this issue, we shut down DnaA expression from its native level using the
209 deactivated miniature Un1Cas12f1 (dUn1Cas12f1) system, guided by sgRNA to repress *dnaA*
210 transcription (Fig. 6A). This system effectively diminished *dnaA* transcription to an extremely low
211 level, yet total *oriC* numbers increased fourfold within 90 min, consistent with two rounds of
212 replication initiation (Fig. 6B). These findings demonstrate that halting DnaA synthesis does not
213 immediately abolish replication initiation.

214 Both the titration and switch models predict a close relationship between DnaA activity oscillations
215 and replication initiation(Berger & Wolde, 2022). However, they fail to account for the multiple
216 rounds of initiation observed after DnaA synthesis was shut down. According to the titration model,
217 initiation should cease immediately once DnaA expression is shut down, as the reduction in DnaA
218 concentration would prevent it from reaching the threshold required to trigger new rounds of
219 replication. In contrast, the switch model predicts infinite initiations following the cessation of DnaA
220 expression (Fig. 6C). This is because the cessation of DnaA synthesis only reduce the production rate
221 of DnaA-ATP and had no effect on the conversion rates between DnaA-ATP and DnaA-ADP. As a result,
222 the ratio of DnaA-ATP to DnaA-ADP would temporarily decrease, causing a brief lag before initiation
223 resumes indefinitely (Fig. 6C).

224 The failure of both models prompts us to revisit the regulatory mechanisms of replication initiation.
225 In the titration model, a substantial fraction of DnaA proteins binds to DnaA-boxes along the
226 chromosome, raising the possibility that these bound proteins serve as a reservoir of free DnaA,
227 sustaining replication initiation even after DnaA synthesis ceases. We thus considered the possibility
228 of some extruder(s) alongside DnaA to sense biomass-DNA deviation, and flush DnaA proteins away
229 from the DnaA-boxes, thus releasing free DnaA to dynamically restore DnaA activity, even in the
230 absence of ongoing DnaA synthesis (Fig. 6D).

231 In this proposed "extrusion model", the extruder is constitutively expressed, synthesized at a
232 constant rate throughout the cell cycle, accumulating in proportion to biomass growth, enabling
233 replication initiation when free DnaA concentrations exceed the critical threshold, as described in
234 the titration model(Hansen & Atlung, 2018; Hansen et al., 1991) (Fig. 6D). This model guarantees the
235 long-term coordination of biomass growth and *oriC* abundance, as well as stable oscillations in free
236 DnaA and *oriC* concentrations (Fig. S3 A). Notably, the extrusion model accounts for the persistence
237 of replication initiation and free DnaA oscillations over multiple cell cycles after DnaA synthesis is
238 halted (Fig. 6C; Fig. S3 B). Moreover, since the extruder mitigates the impact of perturbations on
239 DnaA synthesis, the model predicts a quantitative relationship between initiation mass and DnaA
240 expression levels that aligns with experimental observations (Fig. 6E). Furthermore, a stochastic

implementation of the extrusion model shows the lack of correlation between successive replication initiation events (Fig. S3 C), as observed in recent studies (Si et al., 2019; Witz et al., 2019).

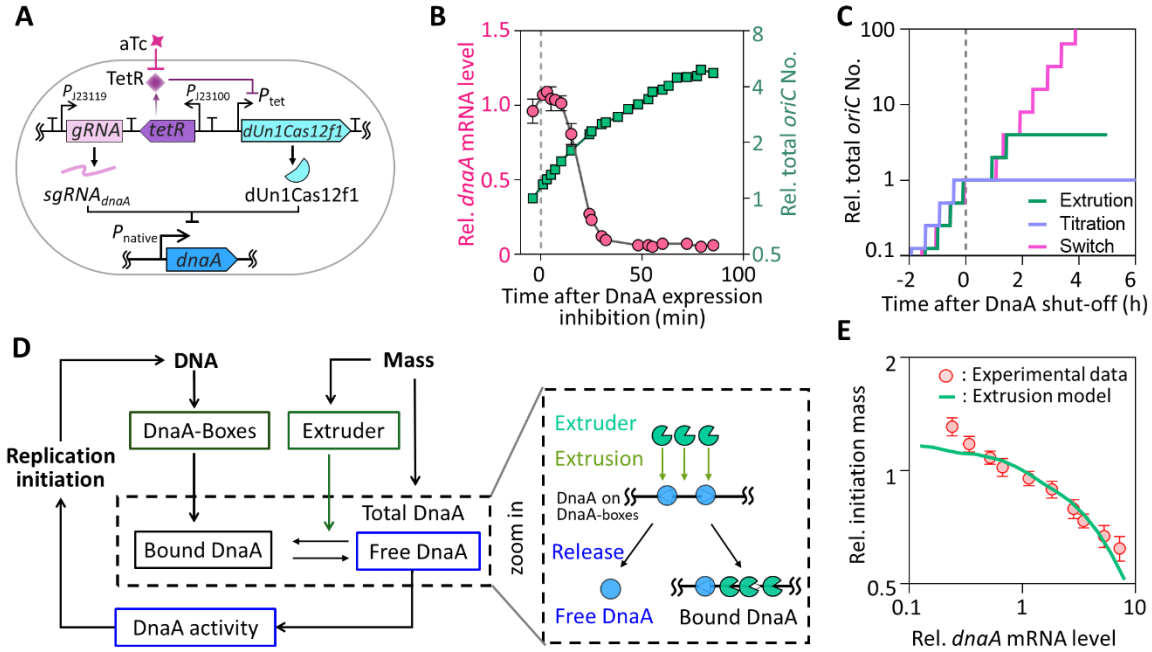

Figure 6. An extrusion model explains DnaA shut-down dynamics. (A) Genetic circuit of the deactivated CRISPR-Cas system for *dnaA* transcription shut-down. *dnaA* gene is targeted by a constitutively expressed sgRNA, while dUn1Cas12f1 expression is inhibited by TetR repressor. These transcription units are separated by terminators. The cassette was integrated into the chromosome near the *oriC* locus. DnaA shutdown is induced by the addition of aTc. **(B)** Time-course of relative *dnaA* mRNA levels (red line, left axis) and total *oriC* number (green line, right axis) following the addition of 50 ng·ml^{-1} aTc at time 0 (dashed line). *dnaA* mRNA levels were normalized to wild-type levels, and *oriC* numbers were normalized to their initial values. Error bars indicate mean ± SD (n = 3 biologically independent experiments). **(C)** Predicted increases in total *oriC* number during *dnaA* transcription shut-down based on three models: the titration model, switch model, and extrusion model. Shutdown was simulated by setting *dnaA* transcription to zero at time 0 (dashed line). **(D)** Schematic of the extrusion model. The model introduces extruder(s) as additional regulators of biomass-DNA coordination, complementing the role of DnaA (left). Increased binding of the extruder to DNA promotes the release of DnaA from DnaA-boxes (right). **(E)** Comparison of the relationship between relative initiation mass and relative *dnaA* mRNA levels from experimental data (Fig. 2F) and predictions of the extrusion model.

Perturbation of H-NS validates the extrusion mechanism

The extrusion model could be validated by changing the expression level of the extruder, which modulates DnaA activity by releasing DnaA from DnaA-boxes. Given their DNA binding properties, NAPs(Dillon & Dorman, 2010) are likely candidates for this extruder role. Therefore, we selected H-NS(Dorman, 2004), a major NAP, which is capable of promoting the release of DnaA from bound DnaA-boxes *in vitro* (Fig. S4), to experimentally assess the validity of the extrusion model. To this end, we constructed a *hns*-titratable strain, incorporating a reporting plasmid to capture changes in DnaA

activity across various H-NS expression levels (Fig. 7A). Under steady-state cultivation, increasing aTc concentrations from 0 to 50 ng·ml^{-1} resulted in *hns* mRNA levels ranging from 0.25 to 5 times the wild-type levels, without affecting growth rate (Fig. S5 A-B). Within this range, DnaA activity increased by approximately 60 % (Fig. 7B), while the initiation mass decreased by 30 % (Fig. 7C; calculated with Fig. 5S C-D), in qualitative agreement with the predictions of the extrusion model (Fig. S5 E-F).

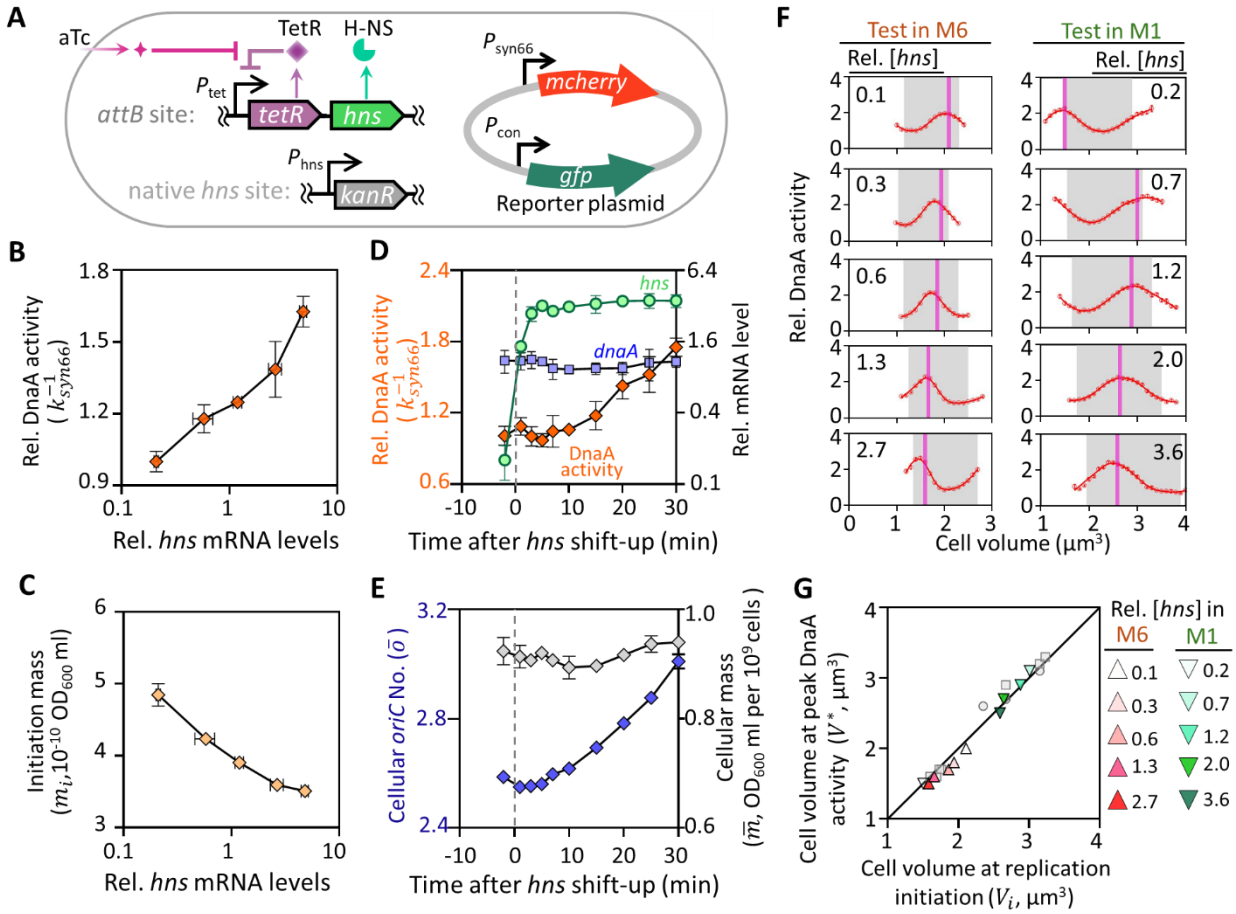

Figure 7. Titration of *hns* expression modulates DnaA activity and replication initiation. (A) Genetic circuit of the *hns*-titratable strain. Expression of *hns* is controlled by a P_{tet}-*tetR* negative feedback loop integrated at the *attB* site, with the native *hns* coding sequence replaced by a kanamycin resistance gene. The plasmid contains P_{syn66}-*mcherry* and P_{con}-*gfp* expression cassettes was used to assess DnaA activity. DnaA activity (**B**) and initiation mass (**C**) were characterized in M6 medium with varying *hns* expression levels during steady-state cultivation. **(D)** mRNA levels of *hns* (green circles) and *dnaA* (blue squares) relative to wild-type levels, along with DnaA activity (orange rhombus), were measured during *hns* shift-up. *hns* shift-up was induced by the addition of 50 ng·ml^{-1} aTc at time 0 (dashed line), following steady-state cultivation in M6 medium without aTc. **(E)** Dynamics of population-averaged *oriC* number (blue rhombus, left axis) and cellular mass (gray rhombus, right axis) during *hns* shift-up. Data represent mean ± SD from 3 biological replicates (**B-E**). **(F)** Cell cycle-dependent DnaA activity oscillations in *hns*-titratable cells cultivated in M1 and M6 media under varying aTc concentrations. Relative *hns* mRNA levels are indicated for each condition. More than 8,000 cells were analyzed for each condition and error bars show the mean ± SEM. **(G)** Correlation between the volume at maximal DnaA activity (V^*) and the volume at replication initiation (V_i) for *hns*-titratable cells grown in M1 (green down-pointing triangle) and M6 (red up-pointing triangle) media with varying *hns* expression

levels. Data for *dnaA*-titratable cells (gray circles) and wild-type *dnaA*-autoregulated cells (Fig. 5C) are included for comparison.

Since H-NS is a global transcriptional regulator (Hommais et al., 2001), we wonder whether its effect on DnaA activity was mediated through *dnaA* transcription. To test this, we measured DnaA activity and *dnaA* mRNA levels during an H-NS shift-up. Upon addition of 50 ng·ml-1 aTc, *hns* levels increased more than 20-fold within a short period, followed by approximately 80 % increase in DnaA activity, with no significant change in *dnaA* mRNA levels (Fig. 7D). Additionally, cellular *oriC* content increased significantly within 30 minutes, while cell mass remained unchanged (Fig. 7E). These results suggest that the rapid increase in DnaA activity and accelerated replication initiation induced by H-NS upregulation is not driven by changes in *dnaA* transcription.

Leveraging the *hns*-titratable strain, we re-examined the tight correlation between DnaA activity oscillations and replication initiation. In two different growth media with varying *hns* levels, the peak of DnaA activity fluctuations (V^*) shifted in concert with the independently measured volume at replication initiation (V_i) (Fig. 7F). Plotting V^* against V_i, revealed the same equivalency observed in wild-type and *dnaA*-titratable cells (Fig. 7G). Collectively, these results support the notion that DnaA activity oscillations, modulated by extrusion, coordinate DNA replication and biomass growth.

Discussion

In this study, we proposed chromosome-driven DnaA activity oscillations as a post-translational "rheostat" coordinating DNA replication with biomass growth in *E. coli*. By developing a SeqA-independent synthetic promoter reporter (P_{syn66}) on a plasmid, we circumvented confounding factors inherent to native systems (Pountain et al., 2024), thereby achieving the direct quantification of DnaA activity dynamics. Crucially, these oscillations persist when *dnaA* transcription is fixed, operate independently of SeqA-mediated repression, and peak precisely at replication initiation across all tested growth conditions. This reveals an essential paradigm: bacteria bypass transcriptional control to synchronize genome duplication with growth through spatial regulation of DnaA-chromosome interactions.

Very recently, Iuliani *et al.* also reported DnaA activity oscillations (Iuliani et al., 2024), which is a significant milestone, innovatively using a chromosomal promoter-reporter system and microfluidics for single-cell DnaA activity observations. They revealed key relationships between DnaA activity, cell size, and division. Our work, however, differs in multiple ways. Methodologically, we engineered a *dnaA*-titratable strain and synthetic promoters like P_{syn66}, enabling precise *dnaA* expression control and cleaner DnaA activity reporting. Our mRNA FISH approach uniquely compares DnaA activity and transcription at the single-cell level. By decoupling initiation volume measurement from DnaA monitoring, we resolve a 1:1 coupling between DnaA activity thresholds and replication initiation events. Regarding research questions, while Iuliani *et al.* focused on DnaA-cell size-division relationships, we addressed the decoupling of replication initiation from *dnaA* expression with our novel extrusion model.

Recently, an integrated "titration-switch" model has been proposed to improve replication cycle stability across different growth rates (Berger & Wolde, 2022; Fu et al., 2023). Although this

integrated model predicts a relationship between initiation mass and *dnaA* mRNA levels that aligns closely with steady-state experimental data (Fig. S6 A), it fails to account for the additional replication initiation observed after *dnaA* shutdown (Fig. S6 B). By incorporating an extruder into this model, we successfully reproduced the additional replication initiation (Fig. S6 C), thus validating the extrusion concept and aligning with experimental observations. These findings highlight the critical role of extrusion in refining our mechanistic understanding of biomass-DNA coordination.

Mechanistically, we propose that NAPs sense biomass-DNA imbalances and extrude DnaA from chromosomal sites, converting physical displacement into biochemical activation, a spatial control strategy mirroring eukaryotic chromatin regulation. H-NS emerges as a prime extruder candidate given its DNA-condensing ability (Dame et al., 2000; Zimmerman, 2006) and replication-timing effects (Fig. 7). This functional multiplicity likely enhances robustness, allowing cells to maintain replication homeostasis despite fluctuating environments, an evolutionary advantage paralleling eukaryotic checkpoint system.

These findings redefine bacterial cell cycle control as a dynamic interplay between physical chromosome remodeling and metabolic sensing. By tethering DnaA activation to biomass accumulation through extrusion, cells achieve a critical feat: noise suppression via spatial filtering of transcriptional fluctuations. Such mechanistic parsimony, using chromosome structure to both store genetic information and regulate replication timing, may represent a fundamental principle of cellular organization. Indeed, parallels to eukaryotic systems are striking: DnaA extrusion resembles ORC licensing through chromatin accessibility (Fragkos et al., 2015), while biomass-DNA coupling evokes yeast size-control checkpoints (Xie et al., 2022).

Future studies could map the complete extruder interactome and elucidate how metabolic signals modulate their activity. Our synthetic reporter system provides a blueprint for dissecting the spatial regulation of DNA-binding proteins, with translational potential in antimicrobial development (targeting pathogen-specific extruders) and synthetic biology (engineering tunable replication circuits). More broadly, this work establishes physical chromosome remodeling as a central coordinator of cellular homeostasis, a concept bridging prokaryotic and eukaryotic cell cycle paradigms.

Materials and Methods

Plasmid and strain Construction

Strains used in this study were derived from *E.coli* MG1655. Information for all strains and plasmids are listed in Tables S1 and S2.

Plasmids for reporting DnaA activity

Plasmids expressing GFP, mCherry, or LacZ under synthetic promoters were constructed based on the pPT plasmid backbone (Zong et al., 2017). The *lacZ* amplified from the MG1655 genome and mcherry gene amplified from pMD19-*hupA-mcherry* plasmid, were assembled into the BspQI/BsrGI-digested pPT backbone via the One Step Cloning Kit (Vazyme, C112), to generate the pPT-lacZ and pPT-RFP plasmids, respectively. Synthetic promoters, generated by annealing the primer pairs listed in Table S3, were ligated directly into the *Bsa*I-digested pPT, pPT-RFP or pPT-lacZ plasmid as required. The native *dnaA* promoter (P_{native}) amplified from the MG1655 genome was digested with *BsaI*, and ligated into the BsaI-digested pPT plasmid. The P_{con}-*gfp* cassette amplified from P_{con}-GFP plasmid was assembled into the SpeI-digested P_{syn66}-RFP plasmid to generate the P_{sny66}-P_{con}-FPs plasmid. Primer information for amplifying DNA fragments is detailed in Table S4.

Plasmids for strain construction

For constructing the plasmid pMD19-Rhns, pMD19-RseqA and pMD19-RdnaA, the *hns*, *seqA* and *dnaA* gene were amplified from MG1655 genome, digested, and ligated into the same enzyme-digested pMD19-tetR plasmid. For constructing the plasmid p15A-RdnaA, the T3-P_{tet}-*tetR-dnaA* cassette, *kan*^{r} gene and p15A-T1 fragment were amplified from plasmidpMD19-RdnaA, pEcCas and PZA31-P_{tet}-M2-GFP, respectively, and then assembled via MultiS One Step Cloning Kit (Vazyme, C113). The plasmid P_CRidnaA1 were obtained by ligating the annealed primer pairs to the *Bsa*I-digested CPP00458 plasmid for the *dnaA* targeting. The chloramphenicol resistance gene *Cm*^{r} amplified from the PZA31-P_{tet}-M2-GFP plasmid replaced the *kan*^{r} gene in the pEcCas plasmid via λRed recombination method, resulting in the CmPcas plasmid. Primer information is detailed in Table S4.

Strain construction

The *seqA*-, and *hns*-titratable strains were constructed as previously described (Zheng et al., 2016). Briefly, after transforming pSIM5 plasmid into MG1655 cells, the P_{tet}-*tetR*-driven *seqA* or *hns* cassette was inserted at the *attB* site on the genome, and then the native gene was replaced with the *kan*^{r} gene amplified from plkml plasmid.

For the construction of *dnaA*-titratable strain, we first inserted the P_{tet}-*tetR cassette* into the *intS* site via CRISPR/Cas9-λRed genome editing system (Jiang et al., 2015) by targeting 20-nucleotide sequence (tcttcctgcagaccagatcc). Then applying the λRed recombination systems in the CmPcas plasmid, the *bla*:P_{tet}-*dnaA* cassette amplified from the pMD19-RdnaA plasmid via overlap PCR, was inserted between the *yid*A and *yid*X genes, and the negative P_{native}-*dnaA* was replaced with the T_3-Kan-T_1 cassette amplified from the p15A-RdnaA plasmid.

In order to delete the native *lacZ* gene in the genome of the RdnaA1, Rhns1 and MG1655 cells, the homologous recombination fragment amplified from the genome of CL1 strain, was used to knock out the native *lac* operon via CRISPR/Cas9-λRed editing system (Jiang et al., 2015) by targeting 20-nucleotide sequence (cttccggctcgtatgttgtg).

For the construction of DnaA shut-down strain (CRidnaA1), the P_{J23119}-$sgRNA_{dnaA}$:P_{J23100}-*tetR*:P_{tet}-*dUn1Cas12f1* cassette was amplified from the P_CRidnaA1 plasmid and flanked with homologous sequences to the *asn*A and *via*A gene. This cassette was then inserted into the MG1655 genome using

CRISPR/Cas9-λRed editing system, targeting the 19-nucleotide sequence (aagccgcctgctcagacgc). The CPP00458 plasmid, kindly provided by the Xiongfei Fu lab, contains the Un1Cas12f1 variant, which carries mutations D143R, T147R, D326A, and K330R that abolish its DNA-cleaving activity. However, it retains the ability to bind DNA in a sgRNA-guided manner, thereby inhibiting the expression of the target gene.

All primers for the construction of DNA fragments are detailed in Table S4.

Growth conditions

Cells for strain construction were grown in in Luria-Bertani (LB) medium with appropriate antibiotics: ampicillin (100 μg·ml^{-1}), kanamycin (50 μg·ml^{-1}), spectinomycin (50 μg·ml^{-1}), chloramphenicol (25 μg·ml^{-1}), based on plasmid presents. For titratable strains, 10 ng·ml^{-1} anhydrotetracycline (aTc) was added during strain construction and seed culture preparation. Seed cultures were initiated by inoculating 3–6 individual colonies from an LB agar plate into 14 ml round-bottom test tubes containing 2 ml of the desired medium for overnight growth.

For physiological phenotypic characterization, all cells were cultivated at 37°C with shaking at 150 rpm in a water bath shaker. The *dnaA*-, *seqA*- and *hns*-titratable cells were characterized under varying aTc concentrations in rich defined medium supplemented with glycerol (M6). *hns*-titratable cells were also characterized in rich defined medium supplemented with glucose (M1). When strains contained reporter plasmid, 25 μg·ml^{-1} chloramphenicol was added. The autoregulated-*dnaA* strain (MGCL1) with a reporter plasmid, was tested in seven different media: M1 (MOPS + EZ + AUCG + Glucose), M2 (MOPS + EZ + Glucose), M3 (MOPS + EZ + AUCG + Gluconate), M6 (MOPS + EZ + AUCG + Glycerol), M12 (MOPS + EZ + Glycerol), M13 (MOPS + CAA + Glycerol), and M18 (MOPS + Glucose). Detailed medium compositions were provided previously (Zheng et al., 2020).

Steady-state growth was established as previously described(Zheng et al., 2020) by culturing cells for ~10 generations in exponential growth phase with ~15-fold dilution at OD_{600} ~0.2, using the same medium supplemented with antibiotic or aTc as required. OD_{600} measurements were taken at consecutive time points using a spectrometer (Genesys 10s, Thermo Fisher Scientific), and the growth rate (or doubling time) was calculated by fitting the data to an exponential growth curve. Samples for determination of population-averaged cell mass ($\bar{m}$) and cellular origin number ($\bar{o}$), quantification of mRNA levels, and mRNA fluorescence in situ hybridization (FISH) were collected when OD_{600} reached ~0.2.

Measurements of population-averaged cellular mass ($\bar{m}$), cellular *oriC* number ($\bar{o}$), and initiation mass (m_i)

The population-averaged cell mass ($\bar{m}$), cellular *oriC* number ($\bar{o}$), and initiation mass (m_i) were calculated as described previously(Zheng et al., 2020). Briefly, $\bar{m}$ was determined by dividing the OD_{600} by the cell concentration (OD_{600} ml per 10^9 cells). For cell counting, samples were collected in precooled cell count buffer (0.9% NaCl with 0.12% formaldehyde, filtered with a 0.22 μm filter) and stained with 1 μg·ml^{-1} DAPI in the same buffer. Cell number concentration was measured by counting the DAPI-stained particles using flow cytometry equipped with 405 nm laser (CytoFLEX, Beckman Coulter Life Sciences). The $\bar{o}$ was calculated based on the classical run-out experiments(Zheng et al., 2020). In brief, cell suspensions were treated with 500 μg·ml^{-1} rifampicin and 30 μg·ml^{-1} cephalexin to inhibit new initiation and cell division, respectively, and maintained for 2-3 mass doublings to complete ongoing replication. Cells were fixed with 70% precooled absolute ethanol, and treated with stain buffer (20mM Tris-HCl, pH 8.0, 130 mM NaCl, 10 ng·ml^{-1} DAPI). Using the same flow cytometry, we measured the cellular origin distribution based on DAPI signaling, from which $\bar{o}$ was calculated.

m_i was calculated based on the equation: $m_i = \frac{\bar{m}}{\bar{o}} \times \frac{1}{ln2}$ (Bremer et al., 1979; Si et al., 2017; Zheng et al., 2016).

Screening of the synthetic promoter library

After transforming the reporter plasmid into *dnaA*-titratable cells, the seed culture was cultivated in M6 medium with 10 ng·ml^{-1} aTc, then diluted 1:180 in fresh medium containing either 0.5 or 50 ng·ml^{-1} aTc and cultivated at 37 °C and 800 r.p.m. in a digital thermo-shaker (AOSHENG) using flat-bottom 96-well plates (Corning). Following approximately 4 hours of pre-cultivation, the cultures were diluted 1:180 in fresh medium with the same aTc concentration. The OD_{600} and GFP fluorescence intensity were continuously monitored during cell growth using a Synergy H1 microplate reader (BioTek). The non-fluorescent strain (MG1655) cultured in 180ul of M6 medium for each experiment was used to subtract the background fluorescence. For OD_{600} between 0.1 and 0.2, the repression fold change was calculated by dividing the mean fluorescence intensity per OD_{600} of the cells grown with 0.5 ng·ml^{-1} aTc induction by the corresponding intensity for cells grown with 50 ng·ml^{-1} aTc induction.

Quantitative real-time PCR

Quantitative real-time PCR was performed using a protocol similar to previously described(Zheng et al., 2016). Briefly, RNA was stabilized using Bacteria Protect Reagent (Qiagen) and extracted using RNeasy mini kit (Qiagen). 500 ng RNA was reverse transcribed (TAKARA), and the resulting cDNA samples were diluted 1:25 with PCR-grade water. Quantitative real-time PCR was carried out on a qTower3 (Analytikjena) or CFX Connect system (Bio-Rad), using the following program: 30 s at 95 °C, followed by 40 cycles of denaturation (5 s at 95 °C), annealing, and elongation (30 s at 58 °C). Primer sequences were listed in Table S4. The *rpoA* gene was used as the reference gene.

***lacZ* and *dnaA* mRNA fluorescence in situ hybridization (FISH)**

FISH for *lacZ* or *dnaA* mRNA was preformed using a method similar to previously described(Skinner et al., 2013). Briefly, antisense DNA oligo probes were designed against *lacZ* or *dnaA*, and synthesized with TAMRA labeling at the 3' end. The sequences of probes targeting *lacZ* or *dnaA* are either as previously described(Skinner et al., 2013) or listed in Table S5. 27 ml steady-state growth culture (OD_{600}~0.2) was fixed by direct adding 3 ml of 37 % (vol/vol) formaldehyde, following by incubation for 30 min at room temperature with gentle mixing using a nutator. The fixed cells were collected by centrifugation at 600 g for 8 minutes, and washed twice with 1 ml RNase-free PBS. The cell pellet was resuspended in 300 µl DEPC water, and 700 µl precooled absolute ethanol was added to permeabilize the cells for 1 hour at room temperature in the nutator. After permeabilization, the cells were divided into two equal parts for characterization of *lacZ* or *dnaA* mRNA as needed. Hybridization was performed as described previously(Skinner et al., 2013), with the stringency of the hybridization and wash solutions adjusted by changing the concentration of formamide, 30 % for *dnaA* probes and 40 % for *lacZ* probes. After hybridization, the cells were washed with the appropriate wash solution and prepared for imaging.

Cell imaging and cell size parameters measurement

For imaging, 3 µl of cell suspension was pipetted onto the center of a 24×60-mm coverslip. A thin 1.5 % agarose pad (prepared with 1xPBS) was then placed on top of the cell suspension droplet. Fluorescent and phase images were acquired using an inverted microscope (IX-83, Olympus) equipped with a 100x oil objective (Olympus), an automated xy-stage (ASI, MS2000), and a sCMOS camera (Prime BSI, photometrics). Fluorescence excitation was performed as previously described (Xia et al., 2022). Solid-state lasers (Coherent OBIS: 405–100 LX, 561–100 LS) and Semrock emission bandpass filters (445/40 nm for DAPI and 598/25 nm for RFP) were used for excitation and collecting fluorescent signals.

Images were aligned with phase contrast channel by selecting at least six pairs of common control points and applying a geometric transformation using the MATLAB imwarp function. This allowed for adjustment of the cell masks in the RFP or DAPI channel. A customized ImageJ -based image-processing package, MicrobeJ (v5.13I$_1$) plugin for Fiji (Ducret et al., 2016), was used to contour cells and calculate cell size parameters and fluorescence intensity, including the mean cell width, cell length, and cell area from phase-contrast images. The cell volume was calculated using a cylinder-plus-two-hemispheres geometry. The total RFP intensity, corrected for background subtraction per cell volume, was then used to estimate the concentration of the related mRNA level.

Characterization of cell cycle-dependent fluctuations in DnaA activity

Data filtering was first performed based on the intensity of the DAPI fluorescence signal. To eliminate non-cell regions resulting from incorrect segmentation of the phase contrast images, only DAPI-positive cells were included in the analysis. To further minimize the potential impact of variability in fixation, permeabilization, and wash efficiencies, which could affect the TAMRA fluorescence signal (representing the mRNA FISH signal), only cells with mean DAPI signals within the 95% confidence intervals were included in the subsequent analysis.

The concentration of the *lacZ* mRNA ($[mZ]$) can be expressed as $[mZ] = J/\delta_Z$, where δ_Z is the degradation rate and J is the mRNA synthesis flux. J is in turn given by the promoter on-rate (k), the RNAP concentration ($[RNAP]$), and the concentration of the *lacZ* gene ($[G_Z]$). Assuming that the factors δ_Z, [RNAP], and $[G_Z]$ are the same between the two strains with P_{syn66} and P_{con} driving *lacZ*, then the ratio of the mRNA concentration obtained at each point of the cell cycle gives the ratio of the promoter on-rates, k_{Psyn66} and k_{Pcon}. Since a constitutive promoter is non-responsive to DnaA activity, k_{con} is independent of cell cycle and we can obtain DnaA activity regulated promoter activity as $k_{syn66} = \frac{[mZ](\mathrm{P_{syn66}})}{[mZ](\mathrm{P_{con}})}$, then the DnaA activity is denoted as k_{syn66}^{-1}.

The concentration of the *lacZ* mRNA were binned based on cell volume, with a bin size of 0.1 μm^3, was used to determine $[mZ](P_{syn66})$ and $[mZ](P_{con})$. The relation between $[mZ](P_{con})$ and cell volume was smoothed using the MATLAB smooth function, and from this, k_{syn66} was deduced.

Based on the DnaA activity oscillations, the cell volume where DnaA activity reaches maximum (V^*) was calculated during a representative birth-to-division cell cycle. The cell volume distribution was used to calculate the number of cells in each volume-doubling range. The range containing the highest cells was considered the representative birth-to-division cell cycle and was shaded in gray (Fig. S2 D). From this, V^* was obtained.

Calculation of cell volume at the time of replication initiation (V_i)

Cell volume at the time of replication initiation (V_{init}) was calculated based on population-averaged cell volume ($\bar{V}$), and the population-averaged cellular *oriC* number ($\bar{o}$). The equation used for this calculation is as follows:

$$V_i = v_i \times N_{oriC}^{ini.} = \frac{\bar{V}}{\bar{o}} \times \frac{1}{ln2} \times 2^{\lfloor log_2^{\bar{o}} \rfloor}$$

where v_i is the initiation volume by definition, i.e. cell volume per *oriC* at the time of replication initiation(Bremer et al., 1979; Si et al., 2017; Zheng et al., 2016). $\bar{V}$ was obtained by analyzing the phase contrast images, $\bar{o}$ was obtained by run-out experiments(Zheng et al., 2020). $N_{oriC}^{ini.}$ is the cellular *oriC* number at the time of replication initiation. $\lfloor \log_2 \bar{o} \rfloor$ denotes the floor function of $\log_2 \bar{o}$.

DnaA shut-down experiment

To shut-down DnaA expression, steady-state growth of the CRidnaA1 cells was first established after ~10 generations of exponential growth in M1 medium. At OD_{600} between 0.15 and 0.2, 24 mL of cell

533 culture was transferred to 12 mL of pre-warmed M1 medium containing 150 ng·mL^{-1} aTc to induce
534 dUn1Cas12f1 expression at time 0. Under the guidance of *sgRNA*$_{dnaA}$, the transcription of *dnaA* gene
535 was inhibited. Samples were collected at various time points to determine population-averaged
536 cellular mass ($\bar{m}$), cellular *oriC* number ($\bar{o}$), and to quantify mRNA levels. When the OD_{600} reached
537 around 0.2, the cultures were diluted about 2-fold with pre-warmed M1 medium containing 50
538 ng·mL^{-1} aTc to maintain adequate nutrition. The steady-state growing MG1655 cells in M1 medium
539 were also collected for quantification of wild-type *dnaA* mRNA levels. Three independent
540 experiments were conducted.

541 **H-NS shift-up experiment**

542 The DnaA activity reporter plasmid P_{syn66}-P_{con}-FPs was transformed into the *hns*-titratable strain
543 (Rhns2), and cells were cultivated overnight in M6 medium containing 10 ng·mL^{-1} aTc and 25 μg·mL^{-1}
544 chloramphenicol for seed culture. Seed cultures were washed and grown in the same medium
545 without aTc for ~10 generations of exponential growth. At an OD_{600} of ~0.2, 40 mL of cell culture was
546 transferred to 20 mL of pre-warmed same medium containing 150 ng·mL^{-1} aTc to induce H-NS
547 expression at time 0. Samples were collected at time points -2, 1, 3, 5, 7, 10, 15, 20, 25, and 30 minutes
548 for the determination of population-averaged cellular mass ($\bar{m}$), cellular *oriC* number ($\bar{o}$), and
549 quantification of mRNA levels. Steady-state growing MG1655 in M6 medium were also collected for
550 *hns* mRNA quantification. Three independent experiments were conducted.

551 **Electrophoretic mobility shift assay (EMSA)**

552 The genes encoding *dnaA* and *hns* from the MG1655 genome were individually amplified and cloned
553 into the expression vector pET-28a using primers listed in Table S4. *E. coli* BL21 (DE3) carrying pET-
554 28a-DnaA or pET-28a-H-NS was used for overproduction of His_6-DnaA or His_6-H-NS. For each protein
555 purification, a 1 L culture was induced by the addition of 1 mM IPTG at OD_{600} = 0.4. After 1.5 hours of
556 incubation, cells were harvested by centrifugation (5,000 rpm for 20 min at 4 °C). The pellet was
557 resuspended in 50 ml of buffer A (50 mM Tris-HCl, pH 7.0, 500 mM NaCl, 0.5 mM PMSF, 5 % glycerol).
558 Cell resuspension was lysed on ice for 30 minutes (3 seconds on, 7 seconds off) using a sonicator at
559 4 °C, and cell debris was removed by centrifugation (14,000 rpm for 60 min at 4 °C). Subsequently,
560 the protein was purified from the soluble supernatant by Ni^{2+}-affinity chromatography (HisTrap™ HP
561 Columns; GE Healthcares) with a ÄKTA Pure Protein Purification System. Proteins were collected using
562 gradient elution with buffer B [20 mM Tris-HCl, pH 7.5, 500 mM NaCl, 400 mM imidazole, 5 % glycerol].
563 Eluted proteins were further purified and concentrated by ultrafiltration using Amicon Ultra 10K (for
564 H-NS) and 30K (for DnaA) filters (Millipore). Finally, after overnight dialysis (0.025 μm Membrane
565 Filter; MF-Millipore) at 4 °C, the protein was stored in buffer C [45 mM Hepes-KOH, pH 7.6, 600 mM
566 potassium glutamate, 1 mM DTT, 10 mM magnesium acetate, 0.5 mM EDTA, 20 % glycerol].
567 Judgement by SDS/PAGE with Coomassie Brilliant blue staining, the purity of each protein was >90 %.
568 For the experiments where H-NS acts on the *datA* bound by DnaA, the purified DnaA, *datA* and ATP
569 were first incubated in buffer D (20 mM Tris-HCl, pH 7.5, 150 mM potassium glutamate, 10 mM
570 magnesium acetate, 8 mM DTT) at 20 °C for 10 min. Then the H-NS was added to buffer D (15 μl)
571 which contained DnaA-*datA* complexes and incubated for additional 10 min at 20 °C. The final
572 complexes were separated by electrophoresis in 2 % (wt/vol) agarose gel at 80 V for 70 min in Tris-
573 Borate buffer, followed by staining with SYBR Safe (Invitrogen).

574 **Titration model**

575 In the titration model, we posit that the cell mass grows exponentially according to the differential
576 equation $\frac{dV}{dt} = \lambda V$, where V represents the volume of the cell and $\lambda = 1.54\ hr^{-1}$(corresponding

to doubling time of 27 min) is the growth rate. Concurrently, DnaA protein synthesis occurs at a rate proportional to the cell's mass, described by $\frac{dA}{dt} = \alpha_A V$, with $\alpha_A = 5\, hr^{-1} ml^{-1}$ denoting the synthesis rate per unit volume. The chromosome's structure is abstracted as a vector representing the copy numbers of uniformly distributed sites along its length. Specifically, DnaA-boxes, which are binding sites for DnaA proteins, are quantified by summing the copy numbers at their respective locations. In this model, 300 DnaA-boxes (A_b) are evenly distributed on the chromosome while an additional 100 DnaA-boxes are located near the origin of replication. This arrangement approximates a head-weighted distribution of DnaA-boxes and helps prevent over-initiation(Hansen et al., 1991). Binding of DnaA proteins to these DnaA-boxes allows us to calculate the concentration of free DnaA as $[A_f] = (A - A_b)/V$, under condition of $(A - A_b) \geq 0$. DNA replication commences once the concentration of free DnaA exceeds a critical threshold $[A_f^c] = 10\, ml^{-1}$: $[A_f] > [A_f^c]$. 10 min sequestration time was set after replication initiation to mimic the sequestration time(Campbell & Kleckner, 1990).

To explore the dynamics of the *oriC* number following the cessation of *dnaA* expression, we can set the synthesis rate to be zero $\alpha_A = 0$. To simulate the dependence of initiation mass on *dnaA* expression, α_A varies from $1 hr^{-1} ml^{-1}$ to $64 hr^{-1} ml^{-1}$.

Extrusion model

The extrusion model was formulated following the titration model, with an additional extruder introduced as a protein with constant concentration $H = \alpha_H V$ with $\alpha_H = 100\, ml^{-1}$. The additional extruder competes the DnaA-boxes with DnaA proteins, with higher affinity to DnaA-boxes. So that it can displace DnaA from the DnaA-boxes, leading to a revised calculation for free DnaA concentration as $[A_f] = (A - (A_b - H))/V$, under condition of $(A_b - H) \geq 0$ and $(A - (A_b - H)) \geq 0$.

To get the DnaA repression simulation at the population level, we introduced cell division by the assumption of Cooper and Helmstetter that a cell divides at a constant time ($T_{cyc} = 60$ mins) after DNA replication initiation. Meanwhile, we introduced noises on cell mass growth rate and the DnaA synthesis rate at each cell division: $\lambda = \lambda_0 + \eta\lambda_0$, $\alpha_A = \alpha_0 + \eta\alpha_0$ where $\lambda_0 = 0.66\, hr^{-1}, \alpha_0 = 5\, hr^{-1} ml^{-1}$ and $\eta = 0.1$ representing white noise. Symmetric cell division is used in the simulation for simplicity. This titration extrusion model is robust under various range of parameters.

DnaA-ATP/DnaA-ADP switch model

The switch model was simulated following the LDDR model in Berger *et al.* (Berger & Wolde, 2022). The same formulations of the DnaA-ATP fraction dynamics df/dt (equation 5) and the same parameters were used (Berger & Wolde, 2022). The cell division was determined when f reaches a threshold as defined previously (Berger & Wolde, 2022). To simulate the *dnaA* shut-down, we simply deleted the term of *dnaA* synthesis ($\lambda(1 - f)$).

Titration-switch model and titration-switch-extrusion model

In the integrated model combining titration and switch mechanisms, replication initiation is triggered when the concentration of free DnaA-ATP $[A_{ATP}^f]$ exceeds a threshold $[A_{ATP}^{fc}]$. The concentration of free DnaA-ATP is titrated by the DnaA-boxes on the chromosome as in the titration model, with $[A_{ATP}^f] = (A_{ATP} - A_b)/V$, under condition of $(A_{ATP} - A_b) \geq 0$. The parameters related to the titration dynamics remain consistent with those described in earlier sections of titration model.

The dynamics of total DnaA-ATP (A_{ATP}) is governed by both expression and conversion processes as described in Berger *et al*. (Berger & Wolde, 2022). According to this framework, the lipid and DARS systems facilitate the conversion of DnaA-ADP to DnaA-ATP at constant rates, while the *datA* site and

RIDA systems also play a role in converting DnaA-ATP to DnaA-ADP, again at fixed rates. Additionally, the synthesis of new DnaA proteins provides another source of DnaA-ATP. For the parameters governing DnaA-ATP dynamics, we adhere to those specified by Berger *et al.*, ensuring consistency with established research. To get a best fit of the initiation mass-*dnaA* expression relation, high threshold of free DnaA-ATP concentration was applied, $[A_{ATP}^{fc}] = 200\ ml^{-1}$.
To simulate the titration-switch-extrusion model, we incorporated the extruder as described in the extrusion model, where its amount was given by $H = \alpha_H V$. The concentration of free DnaA-ATP was then calculated as $[A_{ATP}^{f}] = (A_{ATP} - (A_b - H))/V$, under condition of $(Abox - H) \geq 0$ and $(A_{ATP} - (A_b - H)) \geq 0$. To explore the best fit of continuous DNA replication rounds following *dnaA* shut-down, $\alpha_H = 400\ ml^{-1}$ is used.

Data availability

All data supporting the findings of this work are available from the corresponding author upon request. Source data are provided with this paper.

Code availability

Simulation data can be generated using the custom-made code and the parameter sets provided. The code is publicly available at https://github.com/BaiYangBqdq/dynamics_of_biomass_DNA_coordination.

Acknowledgements

We thank numerous colleagues for discussions. We sincerely thank Dr. Aiguo Xia for his help with microscopy, and Dr. Sheng Yang for providing valuable suggestions on CRISPR-Cas9 system. Special thanks to Drs. Pan Chu and Yeqing Zong for kindly gifting us the CPP00458 and pPT plasmids. This research was financially supported by the National Natural Science Foundation of China (32025022, 32230062), Strategic Priority Research Program of the Chinese Academy of Sciences (XDB0480000), Joint NSFC-ISF Research Grant (32061143021) to C.L., National Natural Science Foundation of China (32170042), National Key R&D Program of China (2024YFA0916403), Youth Innovation Promotion Association CAS (number 2022369) to H.Z., National Key R&D Program of China (2021YFA0910703) to Y.B.

Author contributions

C.L. and T.H. initiated and directed the research. D.L. and T.W. designed and evaluated the synthetic promoter library and performed mRNA FISH experiments with contributions from C.L. and H.Z. D.L., H.Z. and H.C. characterized the phenotype related to H-NS protein; D.L. and X.H. performed the DnaA shut down experiments; Y.B., H.Z., Z.Z. and T.H. conceptualized the extrusion model and performed the numerical simulations. All the authors analyzed the results and wrote the manuscript.

Competing interests

The authors declare no competing interests.

References

Balakrishnan, R., Mori, M., Segota, I., Zhang, Z., Aebersold, R., Ludwig, C., Hwa, T. 2022. Principles of gene regulation quantitatively connect DNA to RNA and proteins in bacteria. *Science*, **378**(6624), eabk2066. http://doi.org/10.1126/science.abk2066

Berger, M., Wolde, P.R.t. 2022. Robust replication initiation from coupled homeostatic mechanisms. *Nat. Commun.*, **13**(1), 6556. http://doi.org/10.1038/s41467-022-33886-6

Bintu, L., Buchler, N.E., Garcia, H.G., Gerland, U., Hwa, T., Kondev, J., Kuhlman, T., Phillips, R. 2005a. Transcriptional regulation by the numbers: applications. *Curr. Opin. Genet. Dev.*, **15**(2), 125-35. http://doi.org/10.1016/j.gde.2005.02.006

Bintu, L., Buchler, N.E., Garcia, H.G., Gerland, U., Hwa, T., Kondev, J., Phillips, R. 2005b. Transcriptional regulation by the numbers: models. *Curr. Opin. Genet. Dev.*, **15**(2), 116-24. http://doi.org/10.1016/j.gde.2005.02.007

Boye, E., Stokke, T., Kleckner, N., Skarstad, K. 1996. Coordinating DNA replication initiation with cell growth: Differential roles for DnaA and SeqA proteins. *Proc. Natl. Acad. Sci. U. S. A.*, **93**(22), 12206-12211. http://doi.org/10.1073/pnas.93.22.12206

Braun, R.E., O'Day, K., Wright, A. 1985. Autoregulation of the DNA replication gene *dnaA* in *E. coli* K-12. *Cell*, **40**(1), 159-169. http://doi.org/https://doi.org/10.1016/0092-8674(85)90319-8

Bremer, H., Churchward, G., Young, R. 1979. Relation between growth and replication in bacteria. *J. Theor. Biol.*, **81**(3), 533-45. http://doi.org/10.1016/0022-5193(79)90051-1

Campbell, J.L., Kleckner, N. 1990. *E. coli oriC* and the *dnaA* gene promoter are sequestered from dam methyltransferase following the passage of the chromosomal replication fork. *Cell*, **62**(5), 967-79. http://doi.org/10.1016/0092-8674(90)90271-f

Christensen, B.B., Atlung, T., Hansen, F.G. 1999. DnaA boxes are important elements in setting the initiation mass of *Escherichia coli*. *J. Bacteriol.*, **181**(9), 2683-2688. http://doi.org/10.1128/jb.181.9.2683-2688.1999

Dame, R.T., Wyman, C., Goosen, N. 2000. H-NS mediated compaction of DNA visualised by atomic force microscopy. *Nucleic Acids Res.*, **28**(18), 3504-10. http://doi.org/10.1093/nar/28.18.3504

Dillon, S.C., Dorman, C.J. 2010. Bacterial nucleoid-associated proteins, nucleoid structure and gene expression. *Nat. Rev. Microbiol.*, **8**(3), 185-195. http://doi.org/10.1038/nrmicro2261

Donachie, W.D., Blakely, G.W. 2003. Coupling the initiation of chromosome replication to cell size in *Escherichia coli*. *Curr. Opin. Microbiol.*, **6**(2), 146-150. http://doi.org/10.1016/s1369-5274(03)00026-2

Dong, M.J., Luo, H., Gao, F. 2023. DoriC 12.0: an updated database of replication origins in both complete and draft prokaryotic genomes. *Nucleic Acids Res.*, **51**(D1), D117-d120. http://doi.org/10.1093/nar/gkac964

Dorman, C.J. 2004. H-NS: a universal regulator for a dynamic genome. *Nat. Rev. Microbiol.*, **2**(5), 391-400. http://doi.org/10.1038/nrmicro883

Ducret, A., Quardokus, E.M., Brun, Y.V. 2016. MicrobeJ, a tool for high throughput bacterial cell detection and quantitative analysis. *Nat. Microbiol.*, **1**(7), 16077. http://doi.org/10.1038/nmicrobiol.2016.77

Fragkos, M., Ganier, O., Coulombe, P., Méchali, M. 2015. DNA replication origin activation in space and time. *Nat. Rev. Mol. Cell Biol.*, **16**(6), 360-74. http://doi.org/10.1038/nrm4002

Fu, H., Xiao, F., Jun, S. 2023. Bacterial replication initiation as precision control by protein counting. *PRX Life*, **1**(1). http://doi.org/10.1103/prxlife.1.013011

700 Grimwade, J.E., Leonard, A.C. 2021. Blocking, bending, and binding: regulation of initiation of
701 chromosome replication during the *Escherichia coli* cell cycle by transcriptional modulators that
702 interact with origin DNA. *Front. Microbiol.*, **12**. http://doi.org/10.3389/fmicb.2021.732270
703 Hansen, F.G., Atlung, T. 2018. The DnaA tale. *Front. Microbiol.*, **9**.
704 http://doi.org/10.3389/fmicb.2018.00319
705 Hansen, F.G., Christensen, B.B., Atlung, T. 1991. The initiator titration model: computer simulation of
706 chromosome and minichromosome control. *Res. Microbiol.*, **142**(2), 161-167.
707 http://doi.org/https://doi.org/10.1016/0923-2508(91)90025-6
708 Hommais, F., Krin, E., Laurent-Winter, C., Soutourina, O., Malpertuy, A., Le Caer, J.P., Danchin, A.,
709 Bertin, P. 2001. Large-scale monitoring of pleiotropic regulation of gene expression by the
710 prokaryotic nucleoid-associated protein, H-NS. *Mol. Microbiol.*, **40**(1), 20-36.
711 http://doi.org/10.1046/j.1365-2958.2001.02358.x
712 Iuliani, I., Mbemba, G., Lagomarsino, M.C., Sclavi, B. 2024. Direct single-cell observation of a key
713 *Escherichia coli* cell-cycle oscillator. *Sci. Adv.*, **10**(29), eado5398.
714 http://doi.org/10.1126/sciadv.ado5398
715 Jiang, Y., Chen, B., Duan, C., Sun, B., Yang, J., Yang, S. 2015. Multigene editing in the *Escherichia coli*
716 genome via the CRISPR-Cas9 system. *Appl. Environ. Microbiol.*, **81**(7), 2506-2514.
717 http://doi.org/10.1128/aem.04023-14
718 Kaguni, J.M. 2011. Replication initiation at the *Escherichia coli* chromosomal origin. *Curr. Opin. Chem.*
719 *Biol.*, **15**(5), 606-13. http://doi.org/10.1016/j.cbpa.2011.07.016
720 Katayama, T., Kasho, K., Kawakami, H. 2017. The DnaA cycle in *Escherichia coli*: activation, function
721 and inactivation of the initiator protein. *Front. Microbiol.*, **8**.
722 http://doi.org/10.3389/fmicb.2017.02496
723 Khodursky, A., Guzmán, E.C., Hanawalt, P.C. 2015. Thymineless death lives on: new insights into a
724 classic phenomenon. *Annu. Rev. Microbiol.*, **69**, 247-263. http://doi.org/10.1146/annurev-micro-
725 092412-155749
726 Knöppel, A., Broström, O., Gras, K., Elf, J., Fange, D. 2023. Regulatory elements coordinating initiation
727 of chromosome replication to the *Escherichia coli* cell cycle. *Proc. Natl. Acad. Sci. U. S. A.*, **120**(22),
728 e2213795120. http://doi.org/10.1073/pnas.2213795120
729 Løbner-Olesen, A., Skarstad, K., Hansen, F.G., von Meyenburg, K., Boye, E. 1989. The DnaA protein
730 determines the initiation mass of *Escherichia coli* K-12. *Cell*, **57**(5), 881-9.
731 http://doi.org/10.1016/0092-8674(89)90802-7
732 Lu, M., Campbell, J.L., Boye, E., Kleckner, N. 1994. SeqA: a negative modulator of replication initiation
733 in *E. coli*. *Cell*, **77**(3), 413-26. http://doi.org/10.1016/0092-8674(94)90156-2
734 Lutz, R., Bujard, H. 1997. Independent and tight regulation of transcriptional units in *Escherichia coli*
735 via the LacR/O, the TetR/O and AraC/I1-I2 regulatory elements. *Nucleic Acids Res.*, **25**(6), 1203-10.
736 http://doi.org/10.1093/nar/25.6.1203
737 Mäkelä, J., Papagiannakis, A., Lin, W.H., Lanz, M.C., Glenn, S., Swaffer, M., Marinov, G.K., Skotheim,
738 J.M., Jacobs-Wagner, C. 2024. Genome concentration limits cell growth and modulates proteome
739 composition in *Escherichia coli*. *Elife*, **13**. http://doi.org/10.7554/eLife.97465
740 Ohbayashi, R., Hirooka, S., Onuma, R., Kanesaki, Y., Hirose, Y., Kobayashi, Y., Fujiwara, T., Furusawa, C.,
741 Miyagishima, S.-y. 2020. Evolutionary changes in DnaA-dependent chromosomal replication in
742 cyanobacteria. *Front. Microbiol.*, **11**. http://doi.org/10.3389/fmicb.2020.00786
743 Ozaki, S., Katayama, T. 2012. Highly organized DnaA-*oriC* complexes recruit the single-stranded DNA

744 for replication initiation. *Nucleic Acids Res.*, **40**(4), 1648-65. http://doi.org/10.1093/nar/gkr832
745 Pountain, A.W., Jiang, P., Yao, T., Homaee, E., Guan, Y., McDonald, K.J.C., Podkowik, M., Shopsin, B.,
746 Torres, V.J., Golding, I., Yanai, I. 2024. Transcription–replication interactions reveal bacterial
747 genome regulation. *Nature*, **626**(7999), 661-669. http://doi.org/10.1038/s41586-023-06974-w
748 Saggioro, C., Olliver, A., Sclavi, B. 2013. Temperature-dependence of the DnaA-DNA interaction and
749 its effect on the autoregulation of *dnaA* expression. *Biochem. J.*, **449**, 333-341.
750 http://doi.org/10.1042/bj20120876
751 Sekimizu, K., Bramhill, D., Kornberg, A. 1987. ATP activates DnaA protein in initiating replication of
752 plasmids bearing the origin of the *E. coli* chromosome. *Cell*, **50**(2), 259-265.
753 http://doi.org/https://doi.org/10.1016/0092-8674(87)90221-2
754 Si, F., Le Treut, G., Sauls, J.T., Vadia, S., Levin, P.A., Jun, S. 2019. Mechanistic origin of cell-size control
755 and homeostasis in bacteria. *Curr. Biol.*, **29**(11), 1760-1770.e7.
756 http://doi.org/10.1016/j.cub.2019.04.062
757 Si, F., Li, D., Cox, S.E., Sauls, J.T., Azizi, O., Sou, C., Schwartz, A.B., Erickstad, M.J., Jun, Y., Li, X., Jun, S.
758 2017. Invariance of initiation mass and predictability of cell size in *Escherichia coli*. *Curr. Biol.*, **27**(9),
759 1278-1287. http://doi.org/10.1016/j.cub.2017.03.022
760 Skinner, S.O., Sepulveda, L.A., Xu, H., Golding, I. 2013. Measuring mRNA copy number in individual
761 *Escherichia coli* cells using single-molecule fluorescent *in situ* hybridization. *Nat. Protoc.*, **8**(6),
762 1100-1113. http://doi.org/10.1038/nprot.2013.066
763 Speck, C., Weigel, C., Messer, W. 1999. ATP- and ADP-DnaA protein, a molecular switch in gene
764 regulation. *EMBO J.*, **18**(21), 6169-6176. http://doi.org/10.1093/emboj/18.21.6169
765 Witz, G., van Nimwegen, E., Julou, T. 2019. Initiation of chromosome replication controls both division
766 and replication cycles in *E. coli* through a double-adder mechanism. *Elife*, **8**.
767 http://doi.org/10.7554/eLife.48063
768 Xia, A., Zhang, R., Huang, Y., Ni, L., Pu, L., Li, Y., Yang, S., Jin, F. 2022. An adaptive tracking illumination
769 system for optogenetic control of single bacterial cells. *Appl. Microbiol. Biotechnol.*, **106**(19-20),
770 6775-6784. http://doi.org/10.1007/s00253-022-12177-6
771 Xie, S., Swaffer, M., Skotheim, J.M. 2022. Eukaryotic cell size control and its relation to biosynthesis
772 and senescence. *Annu. Rev. Cell Dev. Biol.*, **38**, 291-319. http://doi.org/10.1146/annurev-cellbio-
773 120219-040142
774 Zaritsky, A., Pritchard, R.H. 1971. Replication time of the chromosome in thymineless mutants of
775 *Escherichia coli*. *J. Mol. Biol.*, **60**(1), 65-74. http://doi.org/10.1016/0022-2836(71)90447-5
776 Zheng, H., Bai, Y., Jiang, M., Tokuyasu, T.A., Huang, X., Zhong, F., Wu, Y., Fu, X., Kleckner, N., Hwa, T.,
777 Liu, C. 2020. General quantitative relations linking cell growth and the cell cycle in *Escherichia coli*.
778 *Nat. Microbiol.*, **5**(8), 995-1001. http://doi.org/10.1038/s41564-020-0717-x
779 Zheng, H., Ho, P.-Y., Jiang, M., Tang, B., Liu, W., Li, D., Yu, X., Kleckner, N.E., Amir, A., Liu, C. 2016.
780 Interrogating the *Escherichia coli* cell cycle by cell dimension perturbations. *Proc. Natl. Acad. Sci. U.*
781 *S. A.*, **113**(52), 15000-15005. http://doi.org/10.1073/pnas.1617932114
782 Zimmerman, S.B. 2006. Cooperative transitions of isolated *Escherichia coli* nucleoids: implications for
783 the nucleoid as a cellular phase. *J. Struct. Biol.*, **153**(2), 160-75.
784 http://doi.org/10.1016/j.jsb.2005.10.011
785 Zong, Y., Zhang, H.M., Lyu, C., Ji, X., Hou, J., Guo, X., Ouyang, Q., Lou, C. 2017. Insulated transcriptional
786 elements enable precise design of genetic circuits. *Nat. Commun.*, **8**(1), 52.
787 http://doi.org/10.1038/s41467-017-00063-z